Elsevier Editorial System(tm) for Wear of Materials 2019

Manuscript Draft

Manuscript Number: WOM2019-D-18-00230R1

Title: Modelling the effectiveness of oil lubrication in reducing both friction and wear in a fretting contact

Article Type: Research Paper

Keywords: Fretting; lubricated contact ; Coupled-Eulerian-Lagrangian approach ; wear and friction coefficients

Corresponding Author: Dr. Wenjie Qin, Ph. D.

Corresponding Author's Institution: Beijing Institute of Technology

First Author: Wenjie Qin, Ph. D.

Order of Authors: Wenjie Qin, Ph. D.; Min Wang; Wei Sun; Shipway Philip; Xudong Li

Abstract: Lubrication is often employed in fretting contacts to reduce wear and stresses associated with high friction. Owing to the very small displacements associated with fretting, penetration of lubricating oils into the contact may not be effective. The efficacy of the penetration of the lubricant into the contact is very difficult to observe experimentally, and accordingly, this paper presents a numerical simulation of a lubricated fretting contact using a Coupled-Eulerian-Lagrangian (CEL) finite element method. Meso-scale CEL finite element models are developed to simulate the cylinder-on-flat arrangement used experimentally at the University of Nottingham in which the roughness of contact surfaces is characterized as fractal geometry by the Weierstrass-Mandelbrot (W-M) function. The fluid-solid and solid-solid contact in the lubricated fretting contact are simulated, and from these, wear and friction coefficients are determined. The effects of contact geometry on lubricated fretting contacts and lubricant on fretting wear are modelled and compared with experimental observations. Results indicate that oil lubrication reduces fretting wear and friction effectively in the less-conforming contacts but has little effect in the more-conforming contacts.

WEAR

Confirmation of Authorship

Please save a copy of this MS Word file, complete and upload as the "Confirmation of Authorship" file.

As corresponding author, I Wenjie Qin , hereby confirm on behalf of all authors that:

1) The authors have obtained the necessary authority for publication.
2) The paper has not been published previously, that it is not under consideration for publication elsewhere, and that if accepted it will not be published elsewhere in the same form, in English or in any other language, without the written consent of the publisher.
3) The paper does not contain material which has been published previously, by the current authors or by others, of which the source is not explicitly cited in the paper.

Upon acceptance of an article by the journal, the author(s) will be asked to transfer the copyright of the article to the publisher. This transfer will ensure the widest possible dissemination of information.

Detailed Response to Reviewers

Dear Editors,

The authors wish to thank the reviewer for the very helpful suggestions. According to the comments, our responses are listed in the following table.

No.	*Comments of the reviewer*	*Responses*
1	In section 3.2, it is well know that the use of explicit method in solving contact problems is questionable. Consequently, the implicit dynamics method should be used in an attempt to improve the accuracy of the results.	Thank you very much for your recommendation. It is true that the implicit dynamics method should be used to improve the accuracy of the results, but the Coupled–Eulerian–Lagrangian (CEL) method provided in ABAQUS must implemented by the Explicit General Contact. Nevertheless, the accuracy of the explicit method can be achieved by using adequately small time steps and limiting the maximum time increment less than the critical value. This limitation is added in Section 2.1 using red texts.
2	In section 3.2.1, the elastic assumption is not very convenient and should be justified.	Thank you very much for your comment. Given that only part of the contact load is supported by the solids in the lubricated contact and the yield stress of S132 steel (840 MPa) is relatively high, the plastic deformation is not likely to occur in the contact solids in this study, the flat and cylinder specimens are modelled as elastic bodies. We have given our explanation in section 3.2.1 in red words.
3	Section 3.3.2 should be modified to section 3.2.2.	Thank you very much for your careful examination. We have modified Section 3.3.2 to Section 3.2.2.
4	In section 3.2.2, why did the authors chose triangular elements? It is well know that quadrilateral elements for solving contact problems are much more efficient than triangular elements.	Thank you very much for your comment. Using the triangular element in this study is to fit the geometry of the rough surfaces of the contacting solids better.
5	In section 5, the depth of the scars can not be obtained from the SEM images. Therefore, a quantitative measuring equipment should be used to measure the two-dimensional profiles of the scars.	Thank you very much for your comments. In fact the depth of the scar is examined by the profilometry equipment. The SEM images used in this paper are just to compare the fretting wear scars in the lubricated contact and dry contact. The corresponding statements have been added before Fig. 11, and the caption of Fig. 11 has also been modified.

All the changes/revisions made in the revised manuscript have been highlighted in red colour.

Sincerely,

Wenjie Qin

Highlights:

♦ A novel approach of modeling lubricated contacts using a CEL finite element method.

♦ The efficacy of the penetration of lubricant into the fretting contacts is simulated.

♦ The wear and friction coefficients in a lubricated fretting contact are determined.

♦ The effects of contact geometry on lubricated fretting contacts are simulated.

Modelling the effectiveness of oil lubrication in reducing both friction and wear in a fretting contact

Wenjie Qin [a], Min Wang [a], Wei Sun [b], Philip Shipway [b], Xudong Li [a]

[a] School of Mechanical Engineering, Beijing Institute of Technology, Beijing, 10081, China

[b] Faculty of Engineering, University of Nottingham, Nottingham NG7 2RD, UK

Abstract

Lubrication is often employed in fretting contacts to reduce wear and stresses associated with high friction. Owing to the very small displacements associated with fretting, penetration of lubricating oils into the contact may not be effective. The efficacy of the penetration of the lubricant into the contact is very difficult to observe experimentally, and accordingly, this paper presents a numerical simulation of a lubricated fretting contact using a Coupled–Eulerian–Lagrangian (CEL) finite element method. Meso-scale CEL finite element models are developed to simulate the cylinder–on–flat arrangement used experimentally at the University of Nottingham in which the roughness of contact surfaces is characterized as fractal geometry by the Weierstrass-Mandelbrot (W-M) function. The fluid–solid and solid–solid contact in the lubricated fretting contact are simulated, and from these, wear and friction coefficients are determined. The effects of contact geometry on lubricated fretting contacts and lubricant on fretting wear are modelled and compared with experimental observations. Results indicate that oil lubrication reduces fretting wear and friction effectively in the less–conforming contacts but has little effect in the more–conforming contacts.

* Corresponding Author: qinwj@bit.edu.cn

Keywords Fretting; lubricated contact；Coupled–Eulerian–Lagrangian approach；wear and friction coefficients

1 Introduction

1.1 Lubricated fretting contact

Fretting is a special wear process which occurs in loaded contacts between two bodies when they are subjected to minute oscillations and usually leads to wear and fatigue damage [1]. There are many factors affecting the fretting damage, including contact pressure, tangential force, sliding amplitude, vibration frequency, surface roughness, temperature, surface hardness, lubrication and so on. The most important factor is the coefficient of friction [2].

Lubrication is an effective way to reduce friction. The effect of lubrication has been verified in the sliding contact of many friction pairs. However, owing to the very small displacements, lubricating oil is sometimes difficult to enter the contact interface, and the lubricating oil may be squeeze out even it enters the contact interface (called the self cleaning [3]). A number of reports in the literature that address lubricated fretting wear have argued that wear behaviour is influenced predominately by the ability of lubricant to penetrate contacts [4–6]. The effectiveness of penetration of lubricating oil into the contact will depend upon the geometry of the contact, the nature of the lubricant and the conditions. For example, the conformity of the contact is one of the important factors. In line contacts, lubricant is more likely to enter the contact interference with

smaller contact radius [7].

Because it is difficult to form a full lubricating oil film, a fretting interface is usually in the state of mixed lubrication and boundary lubrication [4, 8]. The contact load is shared by the roughness solid and the lubricating oil of the contact. Therefore, the surface roughness will affect the characteristics of contact interface in fretting [9].

1.2 Finite element simulating of fretting contact

For over one hundred years, fretting has been intensively investigated in the experimental and theoretical research. However, it is difficult to observe the state of lubricating oil between the contact surfaces directly in experiments, and it is also difficult to predict the behaviour of a real fretting tribo-system of complex geometry with surface roughness by theoretical research. With the rapid development of high performance computers and the methods for solving non-linear problems, finite element (FE) analysis has been applied to simulate the fretting process.

For examples, McColl and Ding et al. presented a FE method to simulate both the fretting wear and the evolution of fretting variables with number of wear cycles in a cylinder-on-flat fretting configuration based on Archard's model [10, 11]. Then Ding et al. presented a FE based fretting wear simulation tool which could model complex geometries like spline coupling and incrementally update the contact geometry with material removal [12]. Later, a kinematic hardening (continuum) plasticity model to represent the cyclic plasticity behaviour was used in the FE wear simulation which was employed to study the evolution of the surface and sub-surface fretting variables [13]. Most recently, the local temperature rise in fretting contact due to frictional power dissipation is also simulated by FE method [14, 15]. Furthermore, Cruzado et al. carried out a series of research on the FE based methodology for the prediction wear scars in thin steel wires under fretting wear conditions [16, 17].

The above studies are all aimed at the dry fretting contact without lubrication. The motivation of this paper is to present the methodology of modeling lubricated contacts in fretting contact using FE method. In this method, the roughness of contact surfaces is characterized as fractal surfaces by the Weierstrass-Mandelbrot (W-M) function, and the lubricated contact is simulated by a Coupled–Eulerian–Lagrangian (CEL) approach in which the solid is Lagrangian and the liquid (the lubricant) is Eulerian. According to the cylinder–on–flat arrangement used in the fretting wear experiment at the University of Nottingham, the corresponding CEL FE models are established, the wear and friction coefficients are determined. The effects of contact geometry on lubricated fretting contacts and lubricant on fretting wear in the less–conforming contacts are modelled and compared with experimental observations.

2 CEL approach

2.1 The Lagrangian and Eulerian formulation

An Eulerian coordinate, also called a spatial coordinate, specifies the location of a point in space, which describes the motion of different particles passing through a certain point in space. A Lagrangian coordinate, also called Material coordinates, labels a material point in a body, which describes the motion of a particle following its the motion. Corresponding to Lagrangian coordinates and Eulerian coordinates, there are two kinds of mesh — Lagrangian mesh and Eulerian mesh. In a Lagrangian mesh, the nodes are coincident with material points. In an Eulerian mesh, the nodes are coincident with spatial points.

In the standard Lagrangian description, the mass, momentum, and energy equations are [18]

$$\frac{\partial \rho}{\partial t} + \rho \nabla \cdot \boldsymbol{v} = 0 , \tag{1}$$

$$\rho \frac{D\boldsymbol{v}}{Dt} = \nabla \cdot \boldsymbol{\sigma} + \rho \boldsymbol{b} , \tag{2}$$

$$\frac{De}{Dt} = \boldsymbol{\sigma} : \boldsymbol{D} , \tag{3}$$

where ρ is the density, $\boldsymbol{v}$ is the material velocity, $\boldsymbol{\sigma}$ is the Cauchy stress, $\boldsymbol{b}$ is the body force, $\boldsymbol{e}$ is the internal energy per unit volume and $\boldsymbol{D}$ is velocity strain.

In Eulerian description, the three conservation equations as follows

$$\frac{\partial \rho}{\partial t} + \nabla \cdot \left(\rho \boldsymbol{v} \right) = 0 , \tag{4}$$

$$\frac{D\rho \boldsymbol{v}}{Dt} + \nabla \cdot (\rho \boldsymbol{v} \otimes \boldsymbol{v}) = \nabla \cdot \boldsymbol{\sigma} + \rho \boldsymbol{b} , \tag{5}$$

$$\frac{\partial e}{\partial t} + \nabla (e \boldsymbol{v}) = \boldsymbol{\sigma} : \boldsymbol{D} . \tag{6}$$

The Eulerian governing equations (4) – (6) have the general conservation form

$$\frac{\partial \phi}{\partial t} + \nabla \cdot \left(\boldsymbol{\Phi} \right) = \boldsymbol{S} , \tag{7}$$

whereϕ is the arbitrary solution variable, $\boldsymbol{\Phi}$ is the flux function, and $\boldsymbol{S}$ is the source term. This equation can be divided into two equations

$$\frac{\partial \phi}{\partial t} = \boldsymbol{S} , \tag{8}$$

$$\frac{\partial \phi}{\partial t} + \nabla \cdot \left(\boldsymbol{\Phi} \right) = 0 , \tag{9}$$

which can be then solved sequentially.

The first step (Lagrangian step) is to solve Eq. (8). The second step (Eulerian step) is to calculate the volume of material transported between adjacent elements and adjust the Lagrangian solution variables by the transport algorithms [18, 19]. Explicit dynamic contact analysis is used in the Lagrangian step, and the equation for the motion of a contact system is [20]

$$\boldsymbol{M}\ddot{\boldsymbol{d}} + \boldsymbol{F}^{i} + \boldsymbol{F}^{c} = \boldsymbol{F}^{e} , \tag{10}$$

where $\boldsymbol{M}$ is the diagonal lumped mass matrix, $\boldsymbol{F}^{e}$ is the applied load vector, $\boldsymbol{F}^{i}$ is the internal force vector, and $\boldsymbol{F}^{c}$ is the contact force vector.

In order to obtain accurate results, incremental steps must be adequately small. The maximum time increment must be less than the critical value of the smallest transition time required for a dilatational wave to cross any element in the mesh. The critical value is defined by $\Delta t_{crit} = L^{e} / c_{d}$, in which L^{e} is the length of the smallest element, c_{d} is the wave velocity of the material.

2.2 Motion of fluid interface

In this approach, the solid is Lagrangian and therefore its boundary is just defined by the element edges. Given that fluid elements tend to become ill-shaped resulted from inhomogeneous movements of the mesh points and reflects on the accuracy of the solution, the fluid (the lubricant) is Eulerian in this paper and the volume of fluid (VOF) method is used to reconstruct the fluid

interfaces based on the volumes fractions of the fluids in an element and its neighboring elements. In the VOF method, a volume fraction scalar field, C_k, is defined as Eq. (11) for each fluid k, determining the fraction of volume that occupies within each computational cell [21].

$$C_k = \frac{V_k}{V_c}, \tag{11}$$

where $\boldsymbol{V_k}$ is the volume of fluid k for the cell and $\boldsymbol{V_c}$ is the volume of the entire cell. C_k=0 for cells that do not contain fluid k; C_k= 1 for cells that only contain the kth fluid and $0 < C_k < 1$ if part but not all of a cell's volume is occupied by the kth fluid.

Assuming that the fluids are immiscible and that their movement is defined by a unique velocity field, the interface motion can then be captured by solving the conservation equation derived from Eq. (5) [21]

$$\frac{\partial C_k}{\partial t} + \nabla \cdot (C_k \boldsymbol{v}) = 0, \tag{12}$$

Then the interface normal direction $\boldsymbol{n}$ can be calculated by various methods such as the Young's method or the least-squares volume-of-fluid interface reconstruction algorithm et al. [21, 22].

3 Modeling of oil lubricated fretting contact

3.1 Description of rough surface

In this study, the rough surface is described by fractal geometry because it is characterized by the properties of continuity, nondifferentiability, scale invariance, and self-affinity, and its two-dimensional surface profile height is given by Weierstrass-Mandelbrot (W-M) function [23]

$$z(x) = G^{D-1} \sum_{n=n_1}^{n_2} \frac{\cos 2\pi \gamma^n x}{\gamma^{(2-D)n}}, \quad 1 < D < 2 \tag{13}$$

where D is the fractal dimension ($1<D<2$), G is the fractal scale coefficient, γ ($\gamma>1$) is a constant which controls the density of frequencies in the surface profile and γ=1.5 is typical for most surfaces, n is the fractal scale index and n_1 and n_2 are the lowest and highest cut-off indexes of frequency. Let $\omega=\gamma^n$ is the spatial frequency of the profile, then ω_L is the starting frequency determined by the sample length L as $\omega_L = 1/L$, and ω_U is the upper limit of frequency which is determined by the profile resolution δ as $\omega_U = 1/2\delta$.

The method of determination of fractal dimension D and fractal roughness G described in [15] is used here. As a cylinder–on–flat arrangement (Fig. 1) used in the fretting wear experiment at the University of Nottingham is concerned, the coordinates of the surface profile of the fretting test specimens are obtained via non-contact laser measurement using Mitaka PF-60, which uses a laser autofocus method to determine the co-ordinates of the profile with a resolution of 0.1 μm in height direction and 0.5 μm in lateral direction. The 1 mm length of the measurement data of the cylinder and flat specimens are shown in Fig. 2. As the fretting amplitude is 50 μm and the contact width is less than 100 μm, the width of the rough contact surfaces to be modelled is limited to 300 μm. The modelled 300 μm long profile heights for the cylinder and the flat samples are shown in Fig. 3.

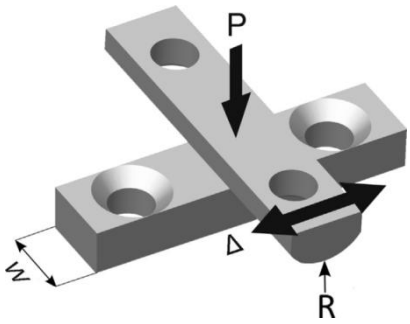

Fig. 1 Cylinder–on–flat specimen arrangement employed in fretting tests [15]

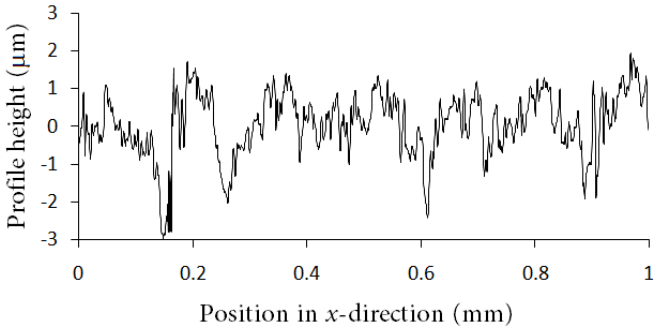

(a)

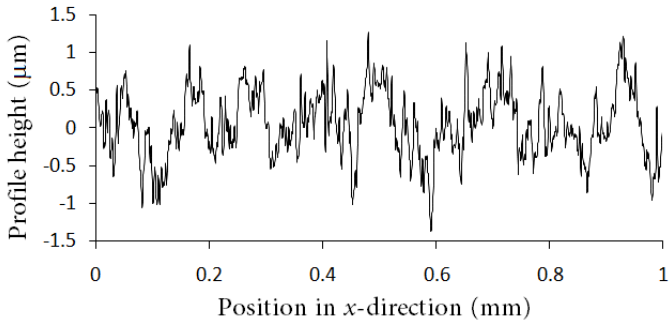

(b)

Fig. 2 Measured profile heights: (a) cylinder surface; (b) flat surface.

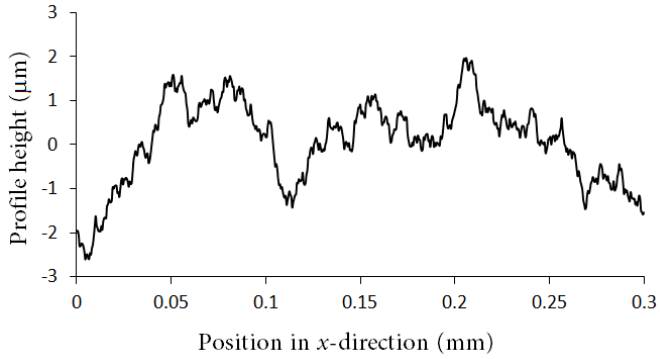

(a)

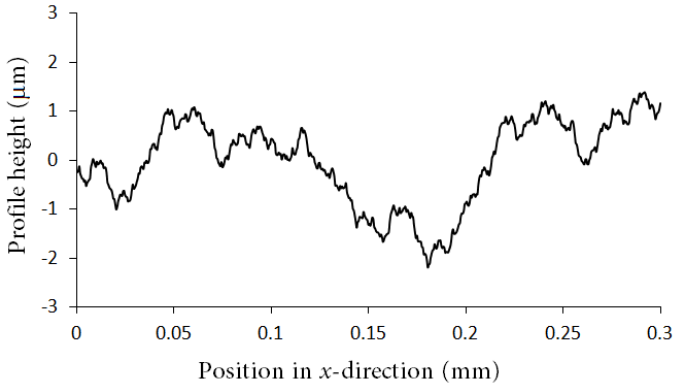

(b)

Fig. 3 Modelled 300 μm long profile heights: (a) cylinder surface; (b) flat surface.

3.2 CEL FE modeling of oil lubricated fretting contact

This study focuses on the modelling of the oil-lubricated fretting contact and simulating the penetration of lubricant into the contact and its effect on the wear. As the cylinder–on–flat arrangement (Fig. 1) is concerned, the contacting specimens are solids and are modelled as the Lagrangian meshes, while the oil lubricant is fluid and is modelled as Eulerian meshes because the flow displacement of the lubricant is large and there is a flow discontinuity when penetration is poor. The explicit dynamics method is applied to simulate the oscillations of the two bodies pressed against each other and the flow of the oil lubricant between the two bodies simultaneously.

3.2.1 Material property

The solid material of the specimens used in the fretting wear experiment is a S132 steel. Given that only part of the contact load is supported by the solids in the lubricated contact and the yield stress of S132 steel (840 MPa) is relatively high, the plastic deformation is not likely to occur in the contact solids in this study, the flat and cylinder specimens are modelled as elastic bodies, and its material property parameters are listed in Table 1.

Table 1. Material properties of S132 steel.

Young's modulus of elasticity E (GPa)	Poisson ratio v	Density ρ_{sol} (kg/m^3)
206.8	0.28	7850

The liquid (the lubricant) material is modelled using the Mie–Grüneisen equation of state (Eq. (14)) with a linear fit assumption for the shock velocity as a function of the particle velocity as Eq. (15) [24, 25].

$$p - p_{ref} = \rho\Gamma(e - e_{ref}), \tag{14}$$

$$U_s = c_0 + sU_p, \tag{15}$$

where p is the pressure, $\boldsymbol{e}$ is the internal energy, p_{ref} and e_{ref} are the reference pressure and internal energy, Γ is the Mie–Grüneisen ratio and $\Gamma = \Gamma_0 \frac{\rho_0}{\rho}$ in which Γ_0 is a material constant and ρ_0 is the reference density , U_s is the shock velocity, U_p is the particle velocity, c_0 is the zero-pressure isentropic speed of sound, and s is a dimensionless parameter which is related to the pressure

derivative of the isentropic bulk modulus. In this study, the parameters s and Γ_0 are simplified to 0 [26]. The material property parameters of the lubricant used in this study are listed in Table 2.

Table 2. Material properties of the lubricant.

Density ρ_{lub} (kg/m^3)	Dynamic viscosity η (Pa•s)	Sound velocity c_0 (m/s)	Mie–Grüneisen ratio Γ	s
880	0.0596	1401	0	0

3.2.2 FE model

The contact between the cylinder and the flat used in the fretting wear experiment is a nonconforming line contact and the contact pressure is concentrated in the zone of a contact width which is investigated here to specify how much is the real area of contact associated with the wear. Since the Eulerian part representing the oil lubricant should be modelled as a three-dimension body in ABAQUS and the sizes of the Lagrangian and Eulerian meshes are very small considering the concentrated contact stress and the thin oil film, the part structures of the cylinder and flat are built up to improve the calculation efficiency in this study. As to one model in which the radius of the cylinder is R=6 mm and the semi–contact–width is 41 μm under the load of 250 N applied on the top surface of the cylinder, the size of the upper specimen is defined as 0.3 mm×0.2 mm×1.0 mm and that of the lower specimen is defined as 0.3mm×0.1mm×1.0mm, more than 20 times the semi–contact–width in the thickness direction. The lubricant is modelled as an Eulerian body. Its height is defined as 6μm, more than the sum of the roughness of the two specimens, and its length and thickness are defined 200μm more than those of the solids to ensure the enough lubrication. Considering the symmetry of the geometry and boundary conditions in the thickness direction, only half the structure is modelled in this study.

The solids are meshed with Lagrangian elements and the lubricant (Eulerian body) is meshed with Eulerian elements (see Fig. 4). The boundary conditions applied to the model includes: the z-symmetric displacement constraint is applied on the middle planes of the model; the bottom of the lower solid is fixed; the load (12.5 N) resulted from that used in the experiment is applied to the top of the upper solid; the oscillating motion with the displacement amplitude of 50 μm and the frequency of 200 Hz along the x direction ($x(t) = 0.05\sin(1256t)(\text{mm})$) is applied to the upper solid; the velocities along the normal directions of the upper and lower surfaces of the Eulerian part in Fig. 4 are set to zero to restrain the lubricant from flowing out of these surfaces; the solid–solid contact constraint is applied between the contacting surfaces of the solids; the fluid–solid contact constraint is applied between the solids and the lubricant.

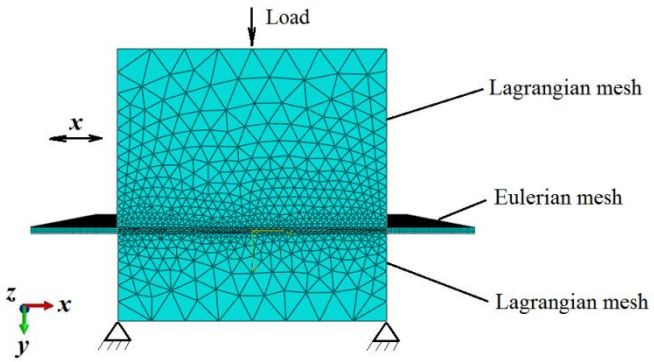

Fig. 4 The mesh model of the assembly

4 Simulation results

4.1 Illustrative results

In the contact zone, 5 μm, 3 μm and 2 μm elements are used to investigate which size of element is required to adequately capture the contact behaviour. Table 3 gives the solid–solid contact stresses resulting from the models with different element sizes in the contact zone at the time of the first reversal of the upper solid. It can be seen that the difference between the contact stresses resulting from the models with 3 μm and 2 μm element sizes in the contact zone is relatively small (the relative difference is about 5%). Therefore, the model with a 3 μm element size in the contact zone is adopted in the simulations in this paper due to the computational efficiency. Fig. 5 shows the solid–solid contact pressure on the top surface of the lower solid resulting from the model with a 3 μm element size in the contact zone at the time of the first reversal of the upper solid.

Table 3. Solid–solid contact stresses resulting from the models with different element sizes in the contact zone.

Element size	5 μm	3 μm	2 μm
Contact stress (MPa)	73.02	225.5	237.9

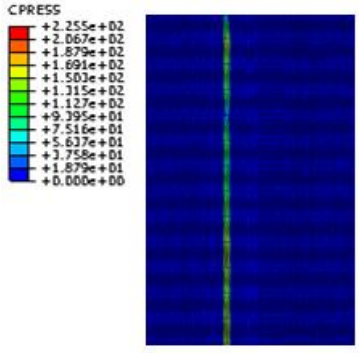

Fig. 5 Solid–solid contact stress.

The solid–solid contact force in one fretting cycle (0.005 s) is investigated as shown in Fig. 6. From this figure, it can be seen that the solids contact occurs before and after the reversals (at t=0.00125 s and t=0.00375 s) since the velocities during these periods are relatively low which result in thinner oil film thickness and cause solid asperity–asperity contact. But the value of contact force is much less that the applied load which is 12.5N. This means that the lubricant has penetrated into the contact area and most of the load is supported by the lubricant. The result can be also verified by the volume fraction results of the fluid (the lubricant) as shown in Fig. 7. At the beginning of the cycle (see Fig. 7 (a)), the volume fraction value in the contact area is greater than zero, which means that there is lubricant all over the contact area. At the first reversal of the upper solid (see Fig. 7 (b)), the volume fraction is zero in some contact area, which means that the lubricant partially penetrated into the contact.

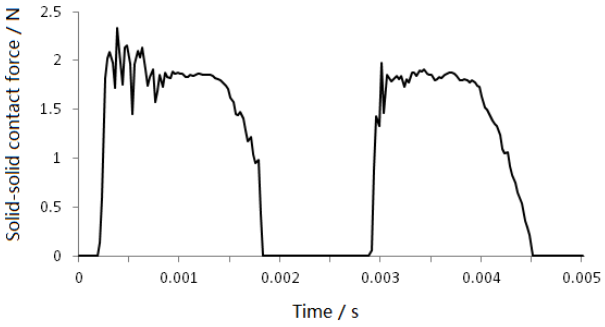

Fig. 6. Solid–solid contact force ratio in one fretting cycle (R=6 mm).

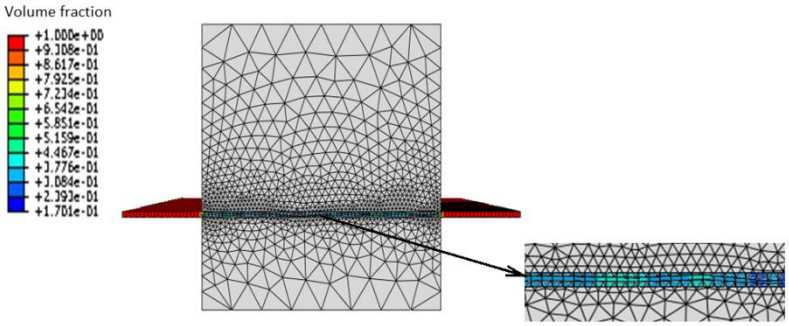

(a)

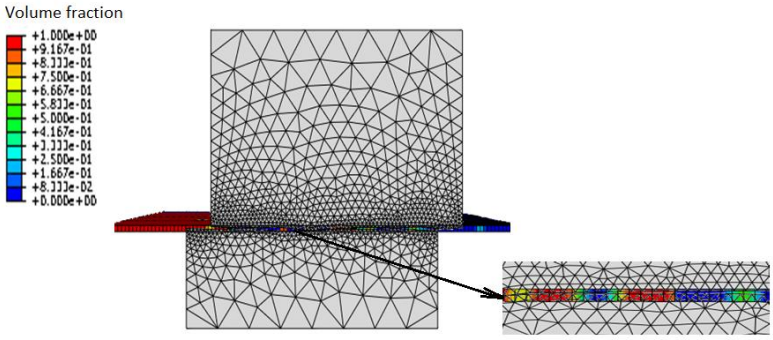

(b)

Fig. 7. The volume fraction results:
(a) at the beginning of the cycle; and (b) at the first reversal of the upper solid.

4.2 Calculation of wear coefficient and friction coefficient

4.2.1 wear coefficient

According to the Archard's model [27], the wear volume can be calculated as

$$V = kPs \tag{16}$$

where k is the dimensional wear coefficient for dry contacts, P is the contact force, and s is the sliding distance.

During the lubricated fretting contact process, wear only occurs in solid–solid contact areas. Since the solid–solid contact force changes with the time, the wear volume is calculated as

$$V = \int_0^T kP_s(t)v(t)dt\,, \tag{17}$$

in which P_s (t) is the solid–solid contact force, v (t) is the sliding velocity and T is the contacting time duration.

Using Eq. (17) to calculate the wear volume in a solid–solid contact as $V = k_l \cdot P \cdot \int_0^T v(t)\,dt$, the wear coefficient for a lubricated contact can be obtained as

$$k_l = V / [P \cdot \int_0^T v(t)\,dt] = \frac{k\int_0^T P_s(t) \cdot v(t)\,dt}{P \cdot T \cdot \int_0^T v(t)\,dt}, \tag{18}$$

From the experiment carried out at the University of Nottingham, the wear coefficient k has been obtained as 2.25×10^{-8} $mm^3N^{-1}mm^{-1}$ in [28]. Using the solid–solid contact force as shown in Fig. 6 and $v(t) = 0.05\cos(1256t)(\mathrm{mm/s})$, the wear coefficient for the lubricated contact is determined as 1.6×10^{-9} $mm^3N^{-1}mm^{-1}$ by Eq. (18).

4.2.2 friction coefficient

In a lubricated contact, the friction is composed of the shearing force of roughness and the viscous resistance of lubricant. The friction coefficient for a lubricated contact is determined by

$$f_l = \frac{fP_s + (A - A_s)\tau_l}{P}, \tag{19}$$

where A is the total nominal contact area, A_s is the solid–solid contact area which can be calculated in ABAQUS software, f is the friction coefficient of the solid–solid contact, and τ_l (t) is the frictional shear stress of the oil film which is defined as

$$\tau_l(t) = \frac{\eta v(t)}{h}, \tag{20}$$

in which h is nominal oil thickness, and η is the dynamic viscosity of the lubricant.

During the lubricated fretting contact process, since the solid–solid contact area A_s is much smaller than the total nominal contact area A, the friction coefficient can be determined approximately by

$$f_l = \frac{f\int_0^T P_s(t)dt + A\int_0^T \frac{\eta v(t)}{h}dt}{P \cdot T}, \tag{21}$$

In this study, the friction coefficient of the solid–solid contact f has been obtained by experiment as 0.89 [28]. Using the solid–solid contact force as shown in Fig. 6, and determining the nominal oil film thickness by the distance between the two nodes which are located at the middle of the upper and lower nominal solid surfaces respectively, the friction coefficient for the lubricated contact is determined as 0.19.

4.3 Efficacy of contact conformity

In order to investigate the effect of contact conformity on fretting wear, the model with the larger radius of the cylinder, which is R=160 mm, is generated to represent the more conforming contact geometry. The other conditions are the same as the model with the cylinder radius of 6 mm. The resulted solid–solid contact force in one fretting cycle is shown in Fig. 8.

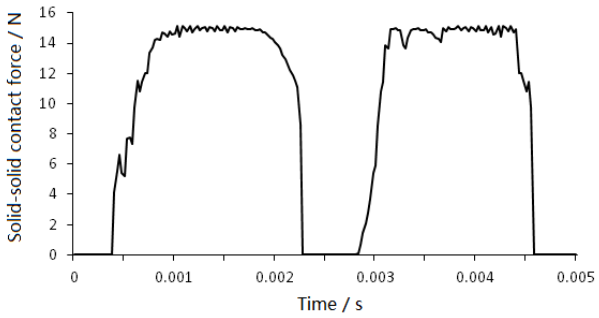

Fig. 8. Solid–solid contact force ratio in one fretting cycle (R=160 mm).

From this figure, it can be seen that the value of solid–solid contact force before and after the reversals is much greater than that with the 6 mm radius cylinder, and even greater than the applied load 12.5 N due to the reversal impact. This means it is difficult for the lubricant to penetrate into the contact area and most of the load is supported by the solid. Adopting the method in Section 4.2, the resulted values of wear coefficient and friction coefficient in lubricated contacts with the 6 mm and 160 mm radius cylinders compared with the experiment values under dry fretting contacts are listed in Tables 4.

Table 4 Wear coefficient and friction coefficient results.

Radius	Wear coefficient / $mm^3N^{-1}mm^{-1}$		Friction coefficient	
R /mm	Lubricated contact	Dry contact	Lubricated contact	Dry contact
6	1.6×10^{-9}	2.25×10^{-8}	0.19	0.89
160	6.0×10^{-9}	8.0×10^{-9}	0.93	1.35

This result shows that the wear coefficient and friction coefficient with the 160 mm radius cylinder is much greater than those with the 6 mm radius cylinder, which are also close to the corresponding values in dry contacts. But both the wear coefficient and friction coefficient with the 6 mm radius cylinder is much smaller than those for dry contacts. Therefore, it can be concluded that the oil lubrication can reduce fretting wear and friction effectively in less–conforming contacts (cylinder with a smaller radius) while has smaller effect on reducing wear and friction in the more–conforming contacts (cylinder with a larger radius).

5 **Simulation of fretting wear**

The effect of the lubricant on reducing wear in less–conforming contacts is investigated by the FE wear simulation.The FE model for the cylinder-on-flat line contact with the 6 mm radius cylinder has been developed with the ABAQUS code to simulate the fretting wear. The contact is simplified to be a two-dimensional plane strain problem and very fine (about 3μm in element size) meshes are generated near the contact zone (see Fig. 9).

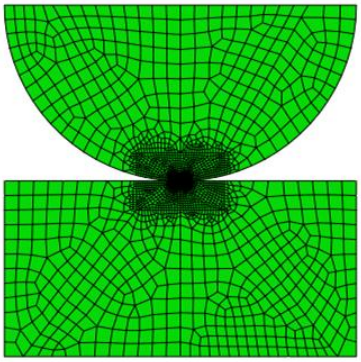

Fig. 9 Two-dimensional FE model for the cylinder-on-flat line contact.

The fretting wear modelling methodology first developed by McColl et al [10] has been applied to the model. Based on Archard's wear law, the incremental local wear depth at each node can be calculated as:

$$\Delta h = kp\Delta\delta\,, \tag{22}$$

where p is the local contact pressure for each node, and $\Delta\delta$ is the incremental local slip distance.

Since most fretting tests have large numbers of cycles, to reduce the computational cost of the simulation, it is assumed that wear is the same in ΔN cycles. Therefore,

$$\Delta h = \Delta N kp\Delta\delta\,. \tag{23}$$

The worn surface geometry is updated incrementally (about 100 times for each fretting cycle) with Arbitrary Lagrangian-Eulerian (ALE) adaptive meshing through a Fortran based ABAQUS user subroutine. Using the wear coefficients for lubricated contacts and dry contacts, the simulated worn profiles of the flat part for 5,000 cycles, 20,000 cycles and 100,000 cycles under the loads of 250 N, the displacement amplitude of 50 μm and the frequency of 200 Hz are illustrated in Fig. 10.

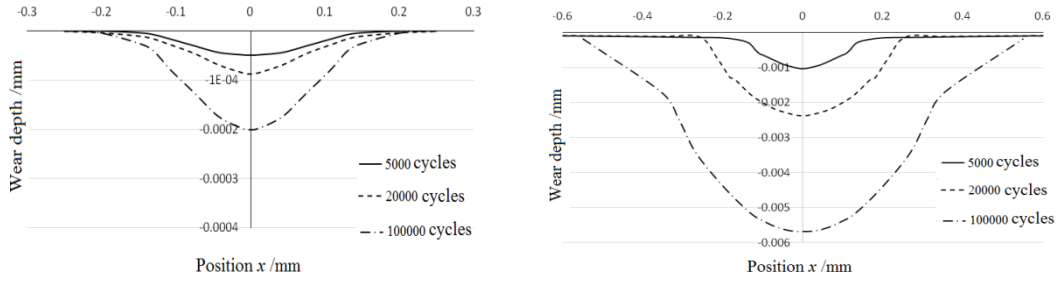

(a) (b)

Fig. 10 Simulated worn profiles of the flat part: (a) lubricated contact; and (b) dry contact.

The results show that the wear depth value of the flat part after 100,000 fretting cycles (0.2 μm) is very small under lubricated condition, while the scar under dry condition is much more significant with the size of about 5.76 μm deep and 1 mm wide. This is close to the tested surface topography results of the wear scars, in which the width of the scar is about 1 mm and the maximum depth of the scare is 6.6 μm under dry condition while the scar under lubricated condition is much slight. The BSE images of the fretting wear scars on the flat specimens are compared in Fig. 11.

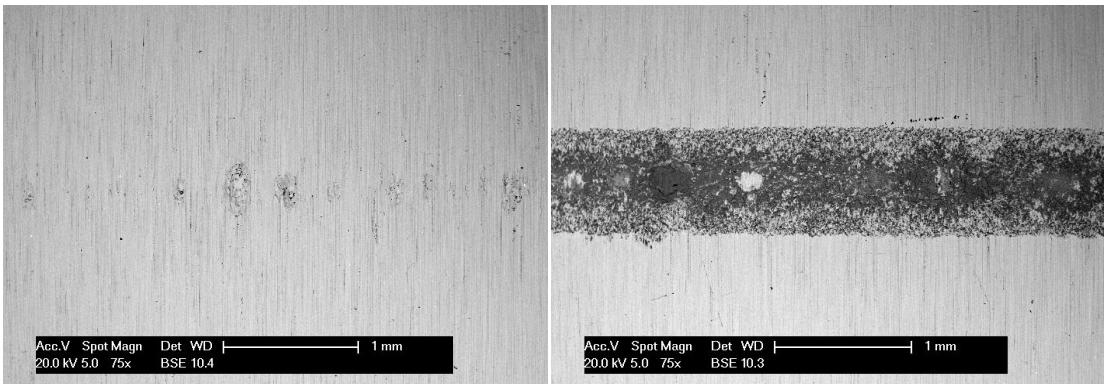

(a) (b)

Fig. 11 Fretting wear scars on the flat part: (a) lubricated contact; and (b) dry contact. [28]

6 Conclusions

This paper presents a methodology of modeling lubricated contacts in fretting wear using a Coupled–Eulerian–Lagrangian (CEL) FE method. As the solid is Lagrangian and the liquid (the lubricant) is Eulerian, the fluid–solid and solid–solid contacts in fretting wear can be simulated and the wear and friction coefficients can be predicted quantitatively. According to the cylinder–on–flat arrangement used in the fretting wear experiment at the University of Nottingham, the corresponding meso-scale CEL FE models are developed and the efficacy of the penetration of the lubricant into the contact is investigated.

The penetration of lubricating oil into the contact is verified by the solid–solid contact forces and the volume fractions of the lubricant, and the effectiveness of the lubricant is found to depend upon the contact conformity. When the cylinder radius is 6 mm corresponding to the less–conforming contact, the solid–solid contact force is much smaller than the applied force and the volume fraction of the fluid is more than zero in most of the contact area. When the cylinder radius is 160 mm corresponding to the more–conforming contact, the value of solid–solid contact force is much greater than that with the 6 mm radius cylinder. This means that the lubricant can penetrate into the contact area effectively and most of the load is supported by the lubricant in less–conforming contacts, while it is difficult for the lubricant to penetrate into the contact area and most of the load is supported by the solid in more–conforming contacts.

The different efficacy of the penetration of the lubricant into the contacts causes that the wear coefficient and friction coefficient with the 160 mm radius cylinder is much greater than those with the 6 mm radius cylinder. Both the wear coefficient and friction coefficient with the 6 mm radius cylinder is much smaller than those for dry contacts. It can be concluded that the oil lubrication can reduce fretting wear and friction effectively in less–conforming contacts but has smaller effects in the more–conforming contacts.

The effect of the lubricant on reducing wear in the less–conforming contacts is investigated by the wear simulation using the FE model for the cylinder-on-flat line contact with the 6 mm radius cylinder. The results show that the wear depth value of the flat part is very small under lubricated condition, while the scar under dry condition is much more significant. The results are consistent with the corresponding experiment results.

Acknowledgements

The authors wish to express their gratitude to the Science and Industry Bureau of China for the financial support to the Powertrain Development Program Grant, under which this research was carried out. Thanks are also due to the workbench provided by the Faculty of Engineering at the University of Nottingham.

References

1. A. Ghosh, W. Wang, F. Sadeghi, An elastic–plastic investigation of third body effects on fretting contact in partial slip, Int. J. Solids Struct. 81 (2016) 95–109.
2. J. M. Dobromirski, Variables of fretting process: are there 50 of them? Stand. Frett. Fatigue Test Methods Equip. 1159 (1992) 60–66.
3. Q. Y. Liu, M. H. Zhu, Z. R. Zhou, G. X. Chen, Effect of the oil-lubricated on fretting characteristics. Chinese Journal of Mechanical Engineering 36 (12) (2000) 1–4.
4. J. Li, Y. H. Lu, Effects of displacement amplitude on fretting wear behaviors and mechanism of Inconel 600 alloy, Wear 304 (2013) 223–230.
5. I. R. McColl, R. B. Waterhouse, S. J. Harris, M. Tsujikawa, Lubricated fretting wear of a high-strength eutectoid steel rope wire, Wear 185 (1995) 203–212.
6. Q. Y. Liu, Z. R. Zhou, Effect of displacement amplitude in oil-lubricated fretting, Wear 239 (2000) 237–243.
7. A. Warmuth, W. Sun, P. H. Shipway, The roles of contact conformity, temperature and displacement amplitude on the lubricated fretting wear of a steel-on-steel contact, Roy. Soc. Open Science 3 (2016) 150637.
8. I. Masaya, Effect of oil supply on fretting wear, Wear 110 (1986) 217–225.
9. K. J. Kubiak, T. G. Mathia, Influence of roughness on contact interface in fretting under dry and boundary lubricated sliding regimes, Wear 267 (2009) 315–321.
10. I. R. McColl, J. Ding, S. B. Leen, Finite element simulation and experimental validation of fretting wear, Wear 256 (11–12) (2004) 1114–1127.
11. J. Ding, S. B. Leen, I. R. McColl, The effect of slip regime on fretting wear-induced stress evolution, Int. J. Fatigue. 26(5) (2004) 521–531.
12. J. Ding, I. R. McColl, S. B. Leen, The application of fretting wear modelling to a spline coupling, Wear 262 (2007) 1205–1216.
13. A. L. Mohd Tobi, J. Ding, G. Bandak, S. B. Leen, P. H. Shipway, A study on the interaction between fretting wear and cyclic plasticity for Ti-6Al-4V, Wear 267 (1–4) (2009) 270–282.
14. X. Jin, W. Sun, P. H. Shipway, The role of geometry changes and debris formation associated with wear on the temperature field in fretting contacts, Tribol. Int. 102 (2016) 392–406.
15. W. Qin, X. Jin, A. Kirk, P.H. Shipway, W. Sun, Effects of surface roughness on local friction and temperature distributions in a steel-on-steel fretting contact. Tribol. Int. 120 (2018) 350–357.
16. A. Cruzado, M. A. Urchegui, X. Gómez, Finite element modeling and experimental validation of fretting wear scars in thin steel wires, Wear 289 (2012) 26–38.
17. A. Cruzado, M. A. Urchegui, X. Gómez, Finite element modeling of fretting wear scars in the thin steel wires: Application in crossed cylinder arrangements, Wear 318 (2014) 98–105.
18. D. J. Benson, S. Okazawa, Contact in a multi-material Eulerian finite element formulation, Comput. Methods Appl. Mech. Engrg. 193 (2004) 4277–4298.
19. B. van Leer, Towards the ultimate conservative difference scheme IV: A new approach to

numerical convection, J. Comput. Phys. 135 (1977) 229–248.
20. M. W. Heinstein, F. J. Mello, S. W. Attaway, T. A. Laursen, Contact-impact modeling in explicit transient dynamics, Comput. Methods Appl. Mech. Engrg. 187 (2000) 621–640.
21. L. Jofre, O. Lehmkuhl, J. Castro, A. Oliva, A 3-D Volume-of-fluid advection method based on cell-vertex velocities for unstructured meshes, Computers & Fluids 94 (2014) 14–29.
22. D. J. Benson, Volume of fluid interface reconstruction methods for multi-material problems, Appl. Mech. Rev. 55 (2) (2002) 151–165.
23. X. Zhang, Y. Xu, R. L. Jackson, An analysis of generated fractal and measured rough surfaces in regards to their multi-scale structure and fractal dimension, Tribol. Int. 105 (2017) 94–101.
24. K. M. Shyue, A fluid-Mixture type algorithm for compressible multicomponent flow with Mie–Grüneisen equation of state, J. of Comput. Phys. 171 (2001) 678–707.
25. Z. Wu, Z. Zong, Numerical calculation of multi-component conservative Euler equations under Mie–Grüneisen equation of state, Chinese Journal of Computer Physics. 28(6) (2011) 803–809.
26. B. Lorentz, A. Albers, A numerical model for mixed lubrication taking into account surface topography, tangential adhesion effects and plastic deformations, Tribol. Int. 59 (2013) 259–266.
27. J. L. Archard, Contact and rubbing of flat surfaces, J. Appl. Phys. 24(8) (1953) 981–988.
28. A. R. Warmuth, The effect of contact geometry and frequency on dry and lubricated fretting wear, University of Nottingham, UK, 2014.

Figure 1

Click here to download high resolution image

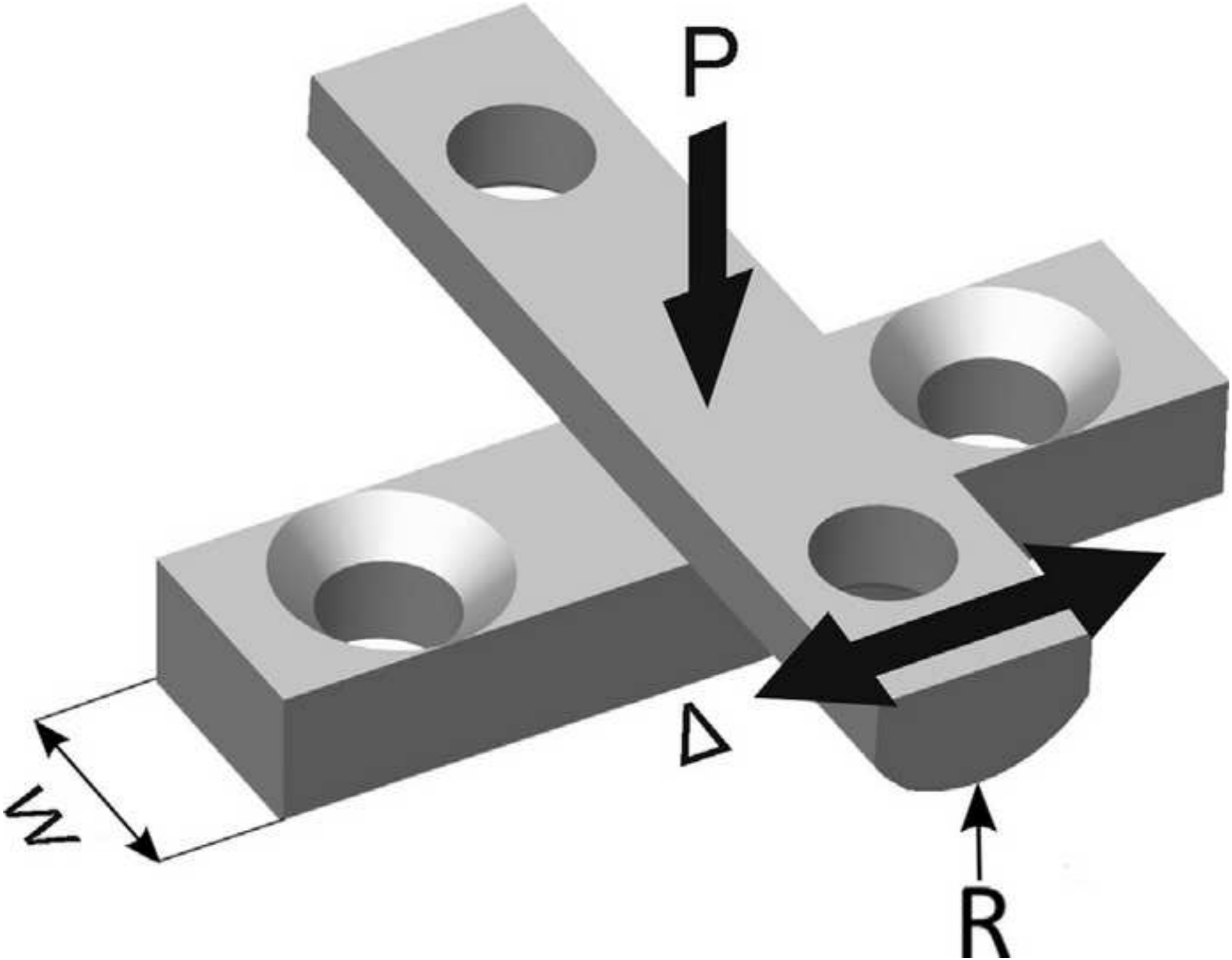

Figure 2(a)

Click here to download high resolution image

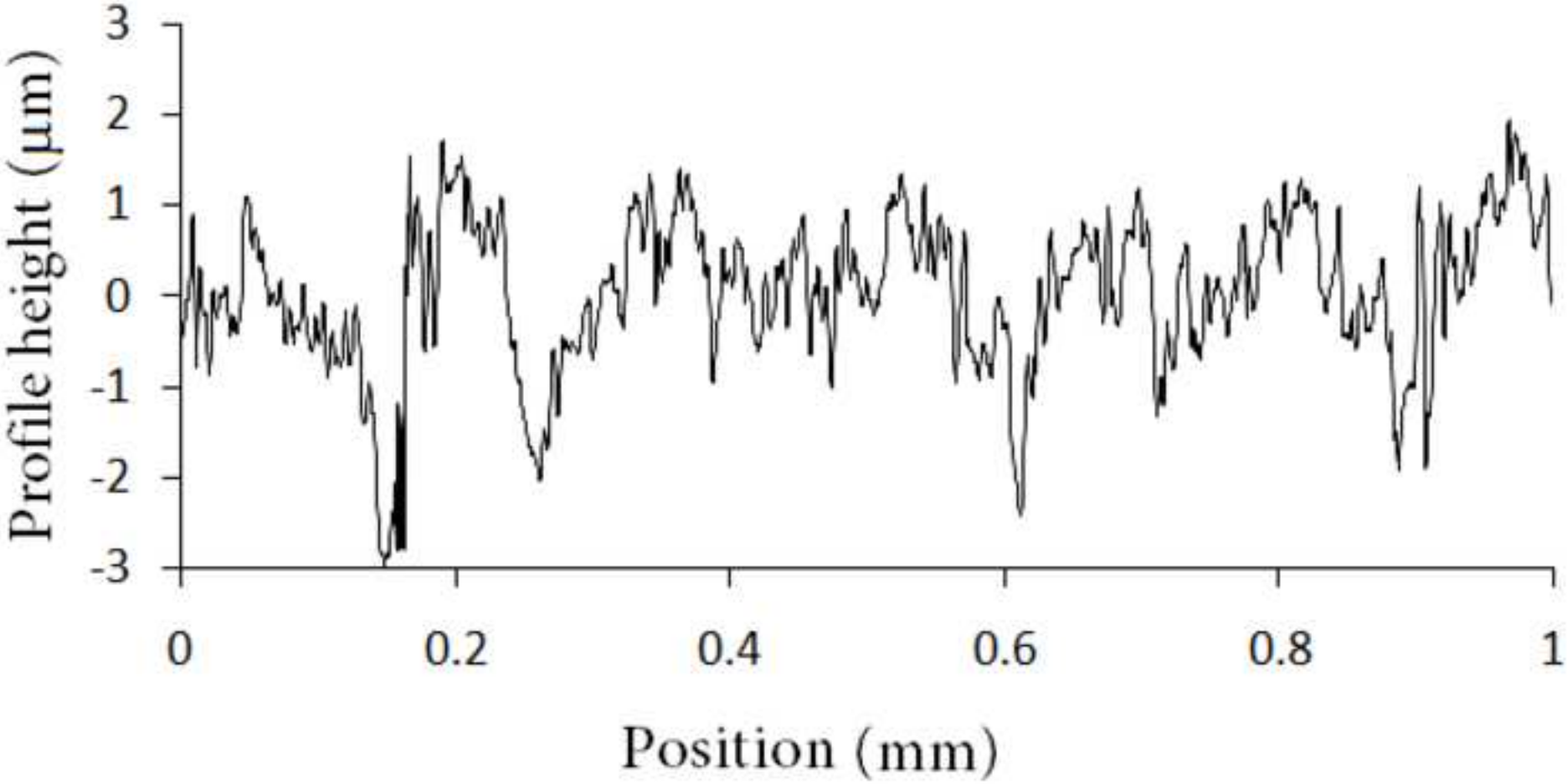

Figure 2(b)

Click here to download high resolution image

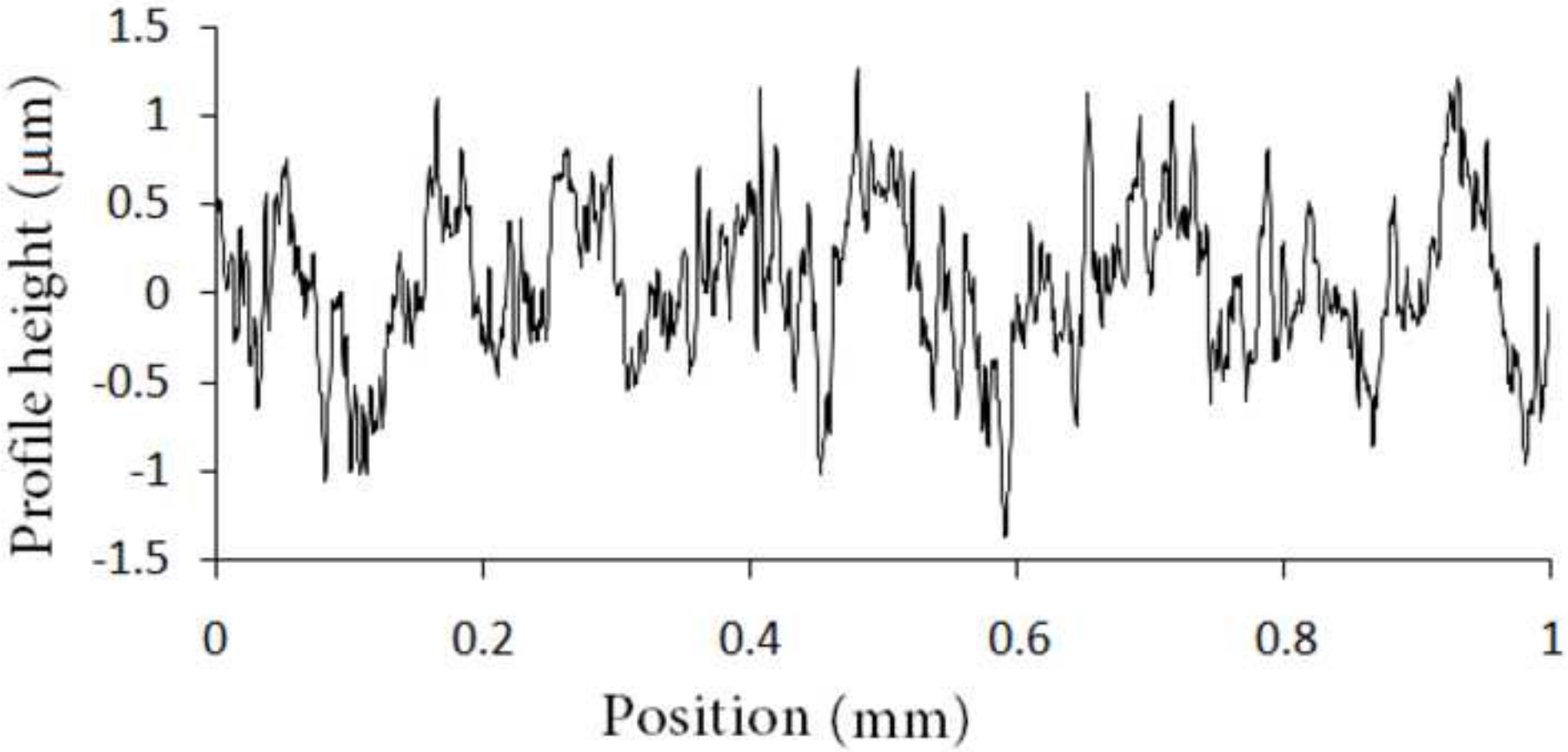

Figure 3(a)
Click here to download high resolution image

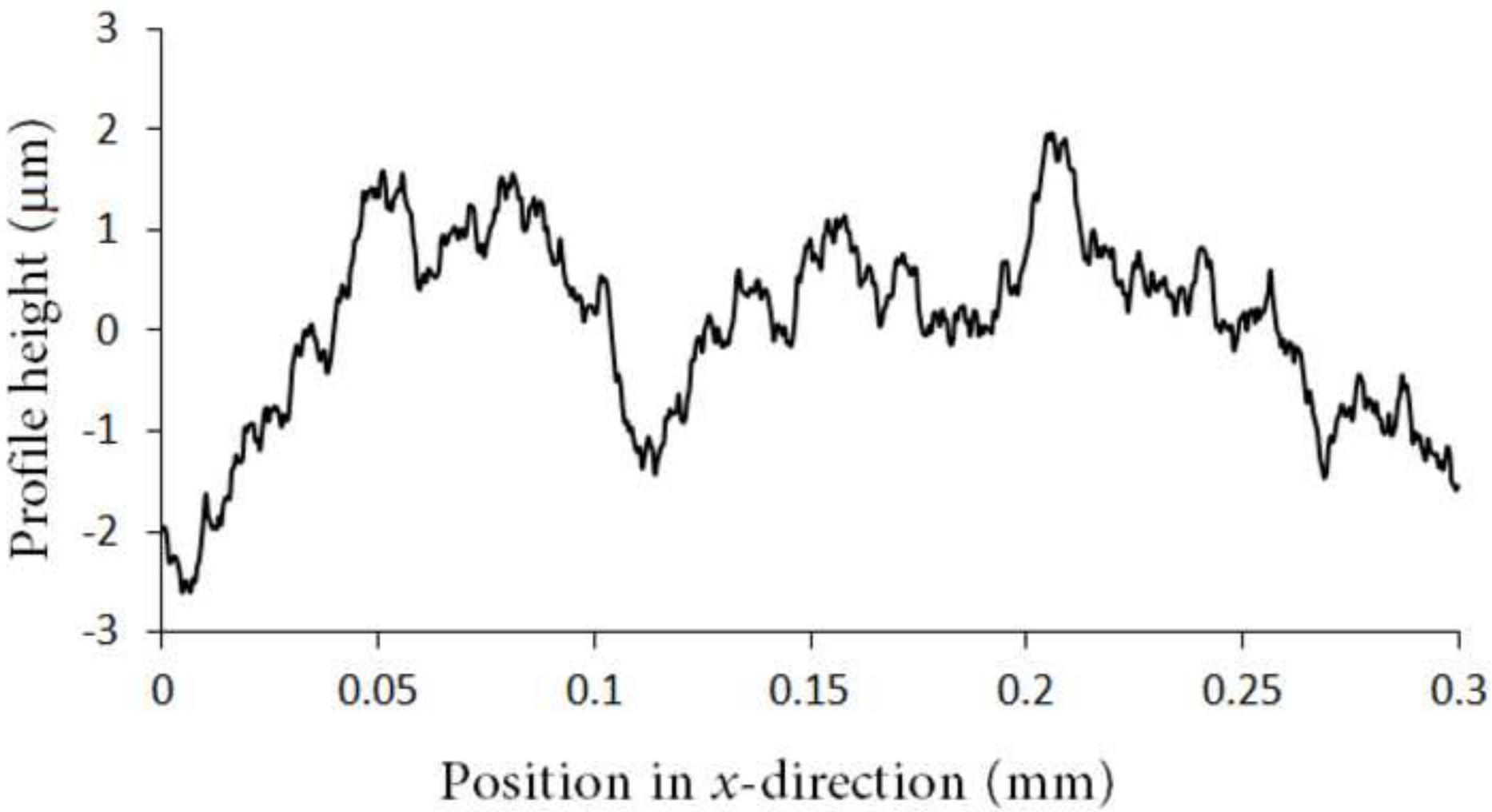

Figure 3(b)

Click here to download high resolution image

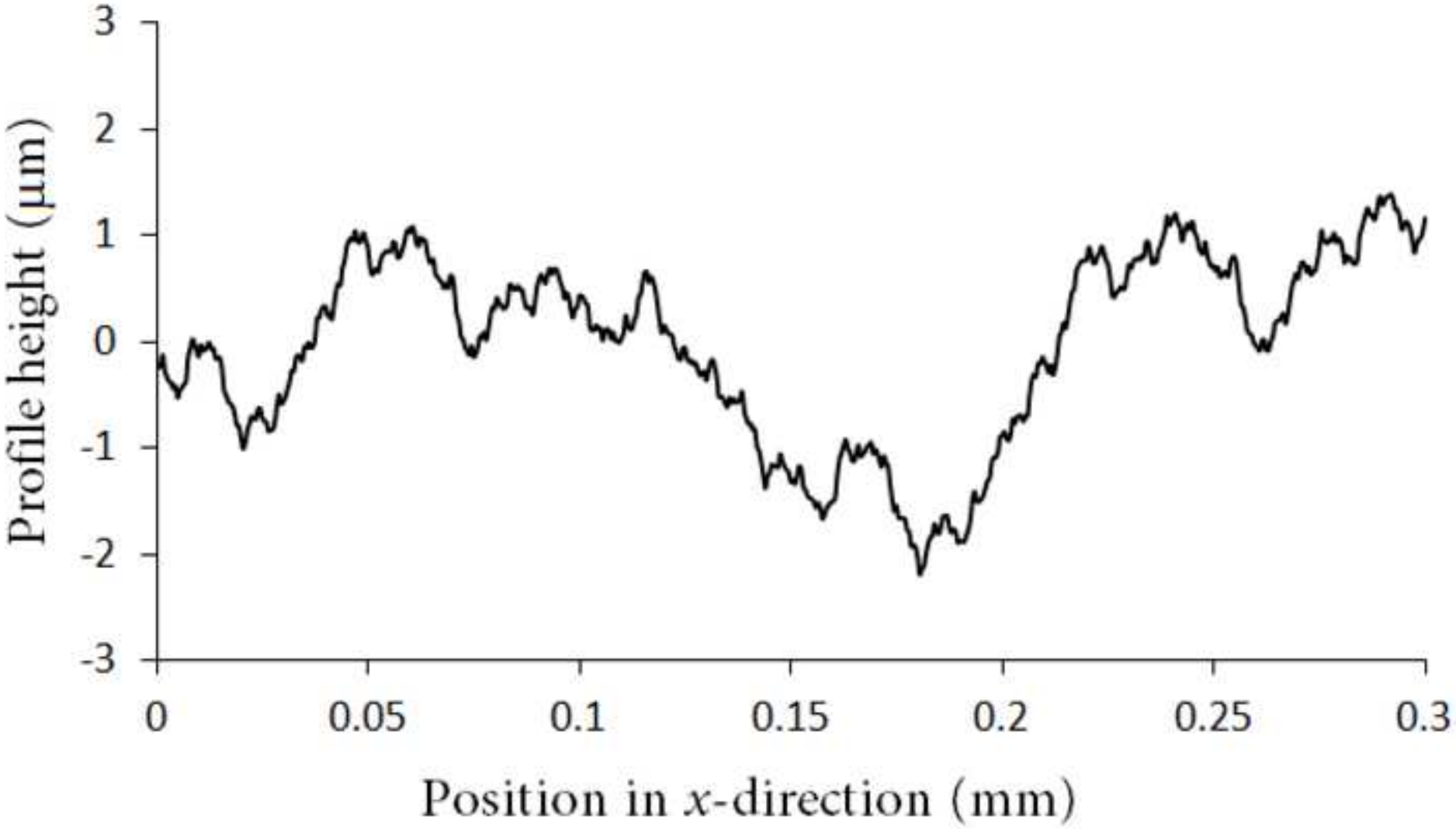

Figure 4
Click here to download high resolution image

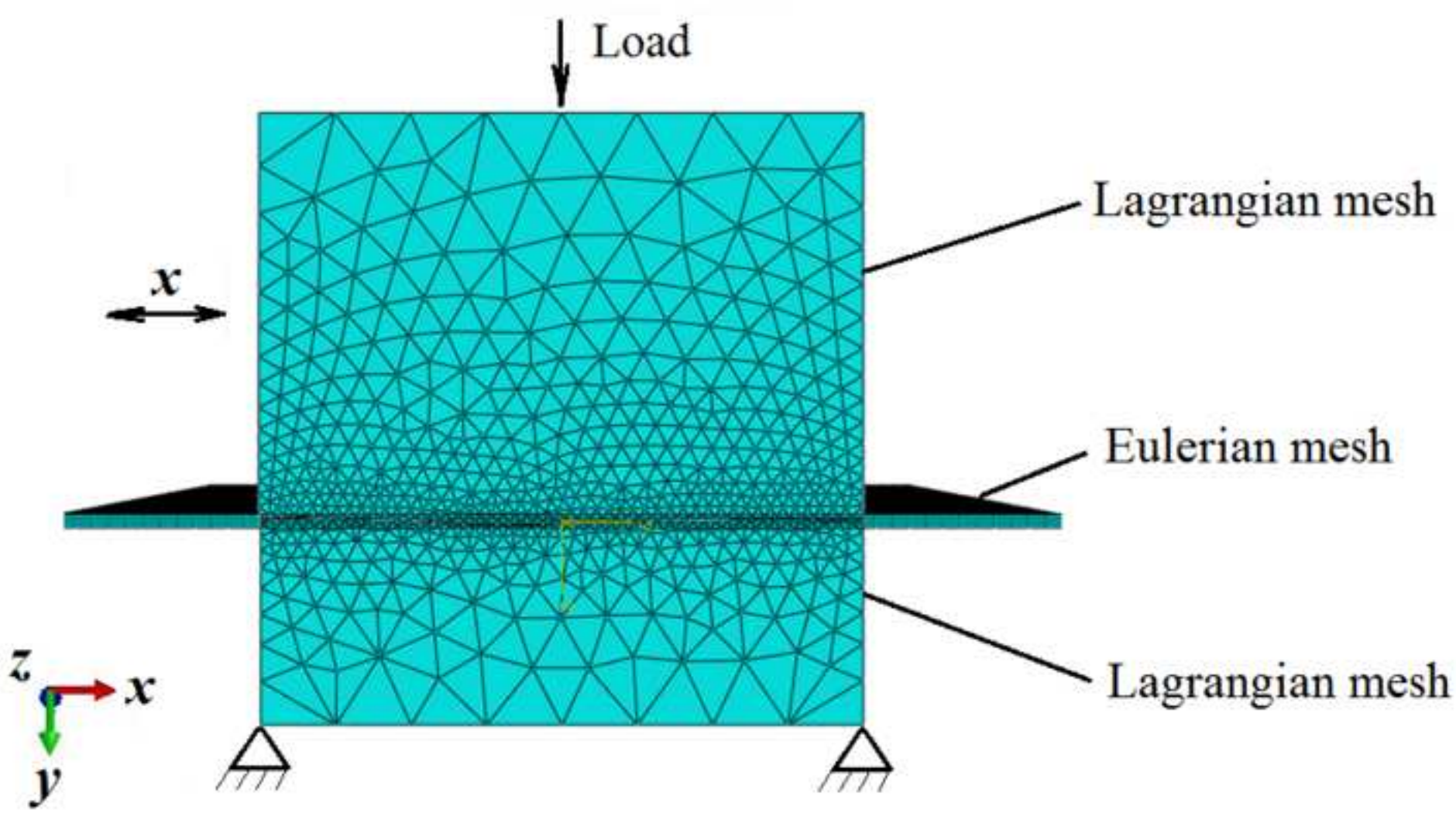

Figure 5

Click here to download high resolution image

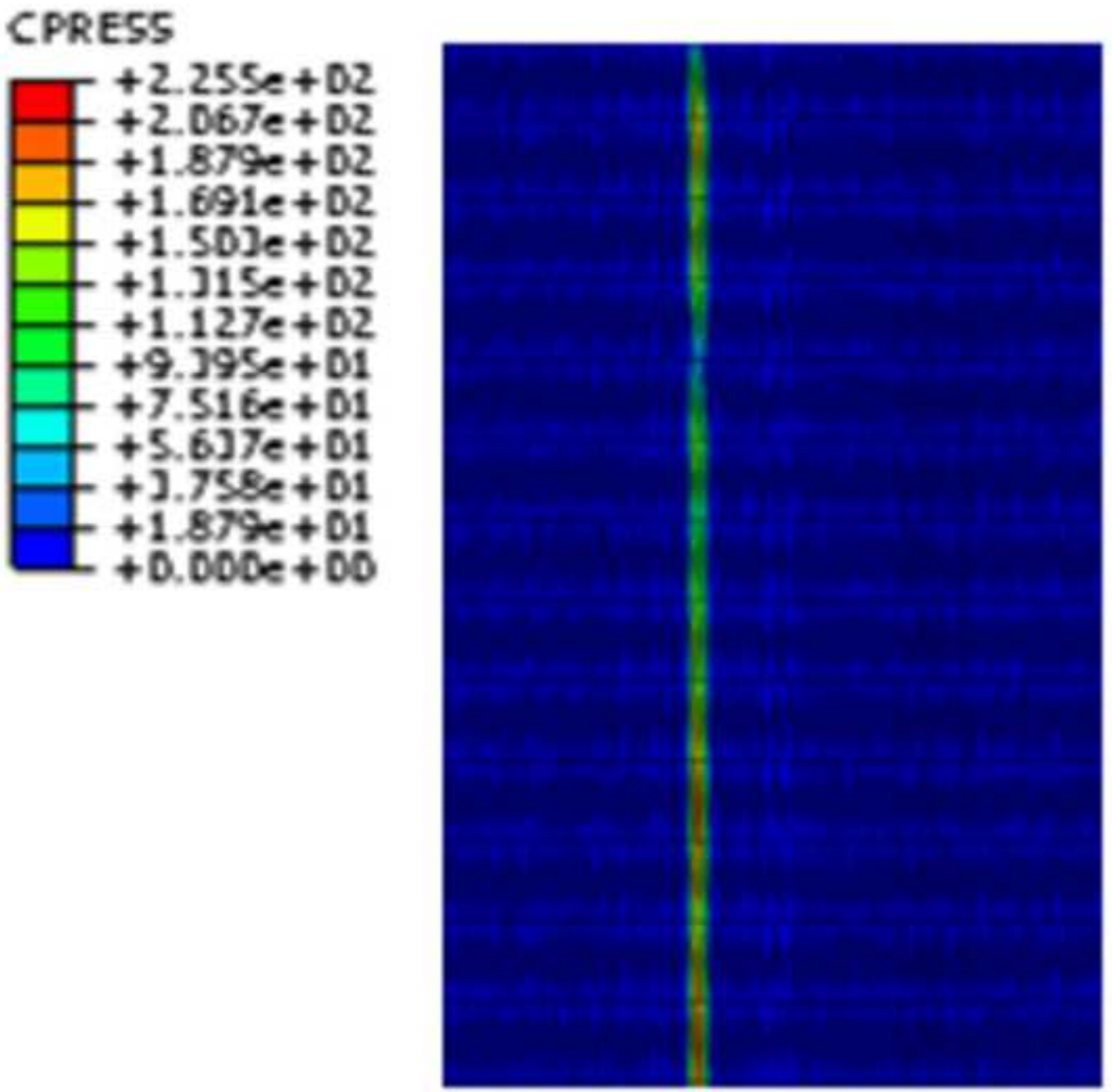

Figure 6
Click here to download high resolution image

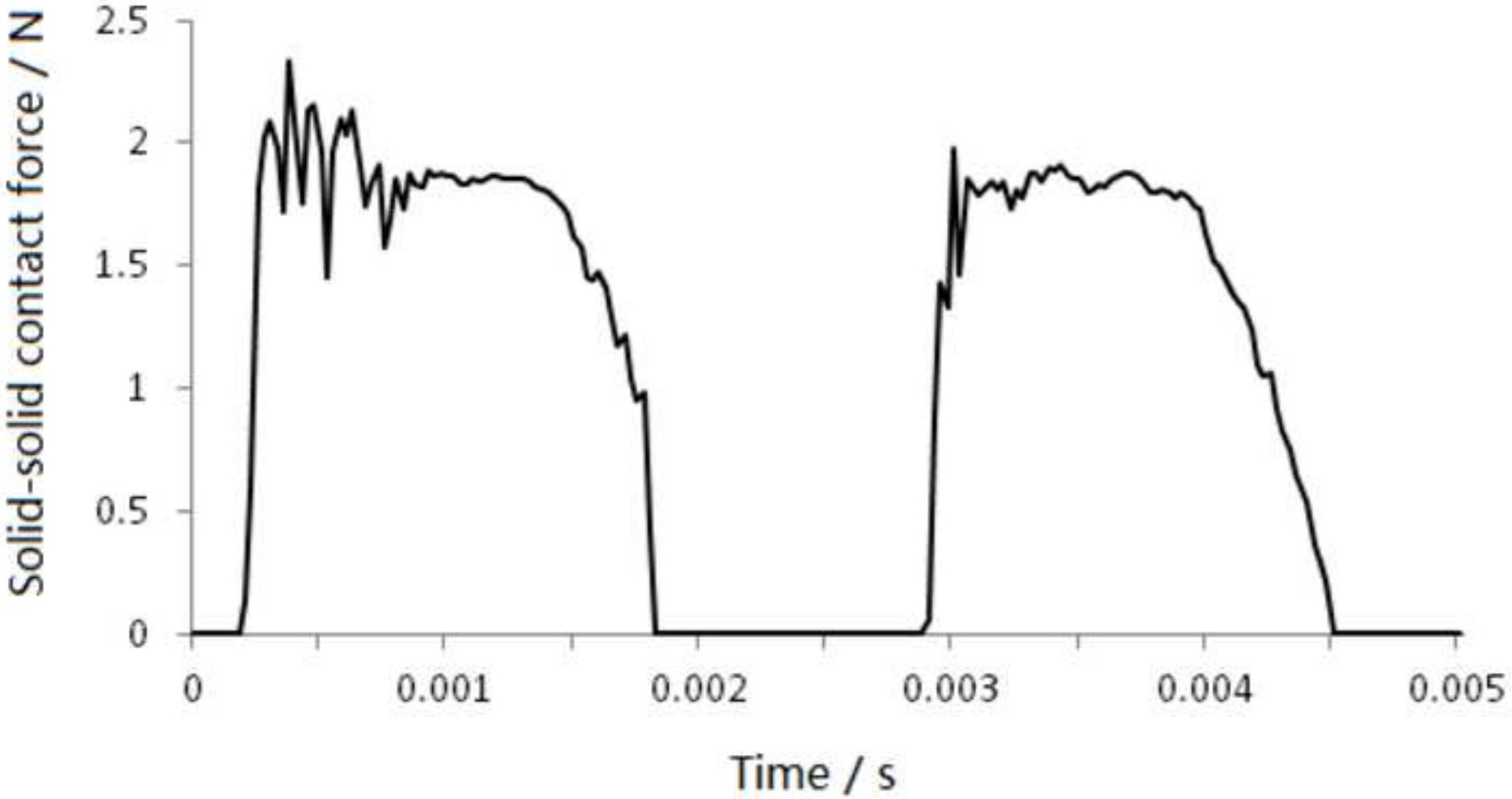

Figure 7(a)

Click here to download high resolution image

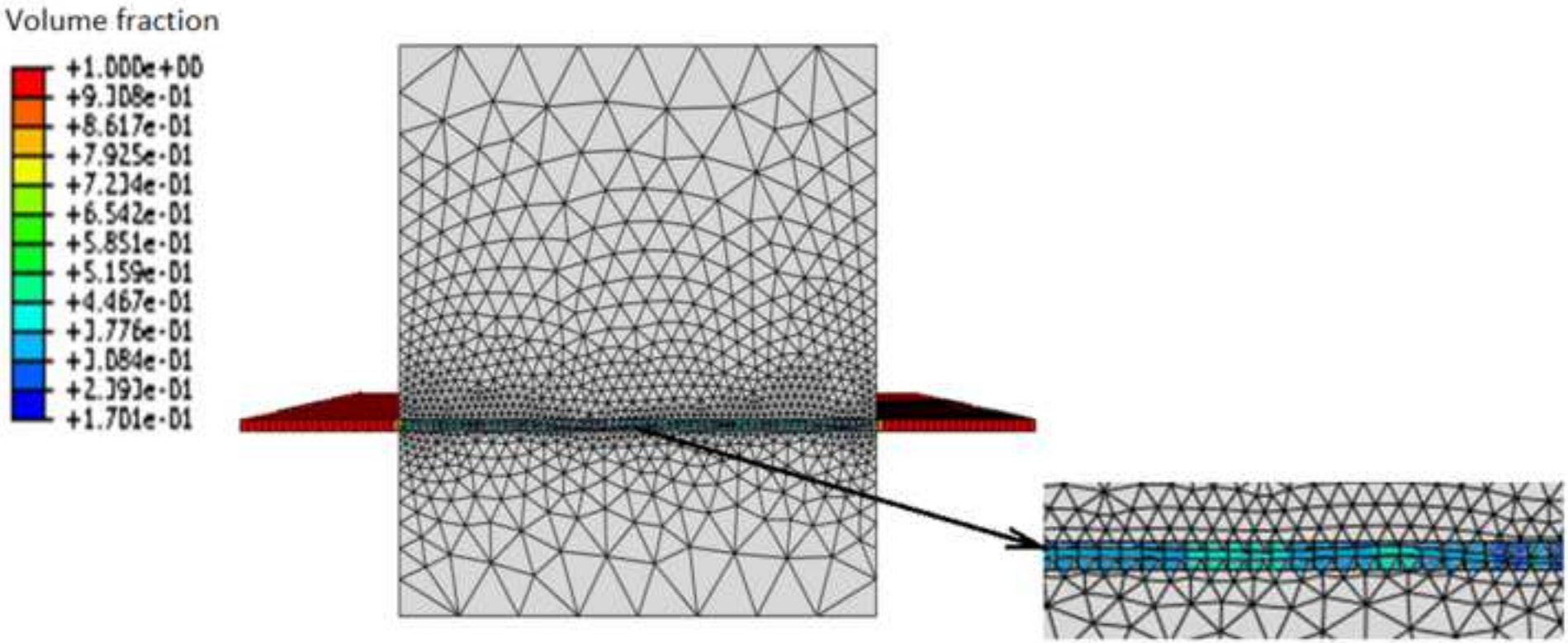

Figure 7(b)

Click here to download high resolution image

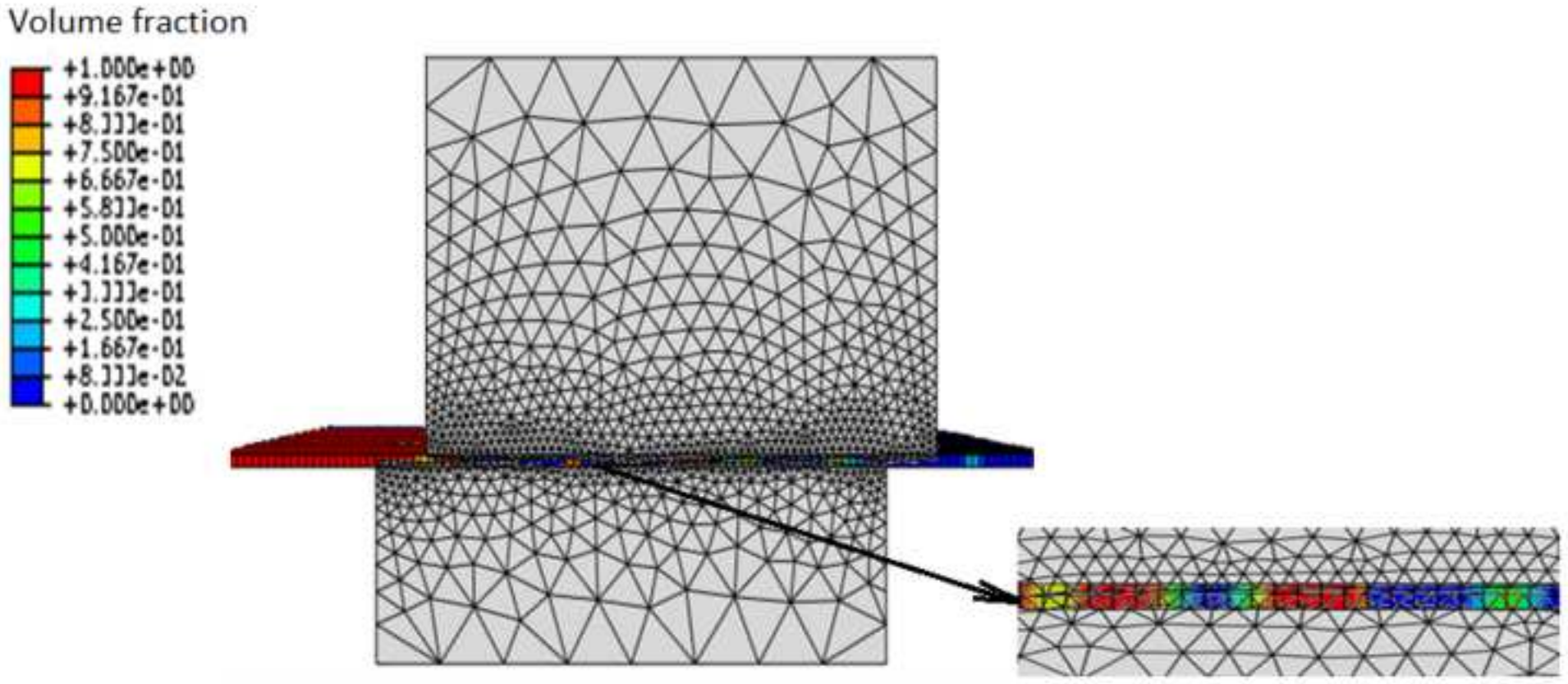

Figure 8

Click here to download high resolution image

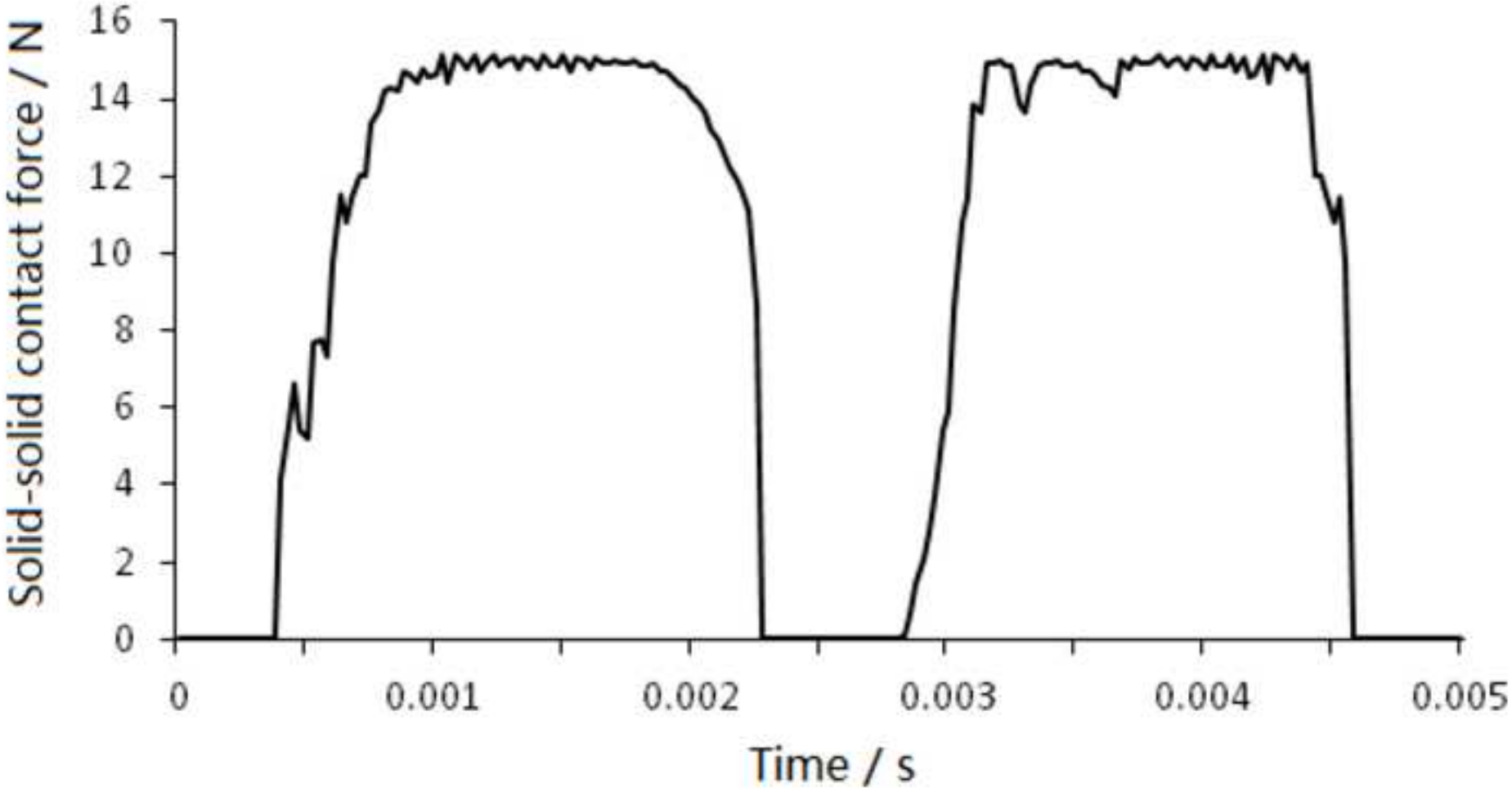

Figure 9

Click here to download high resolution image

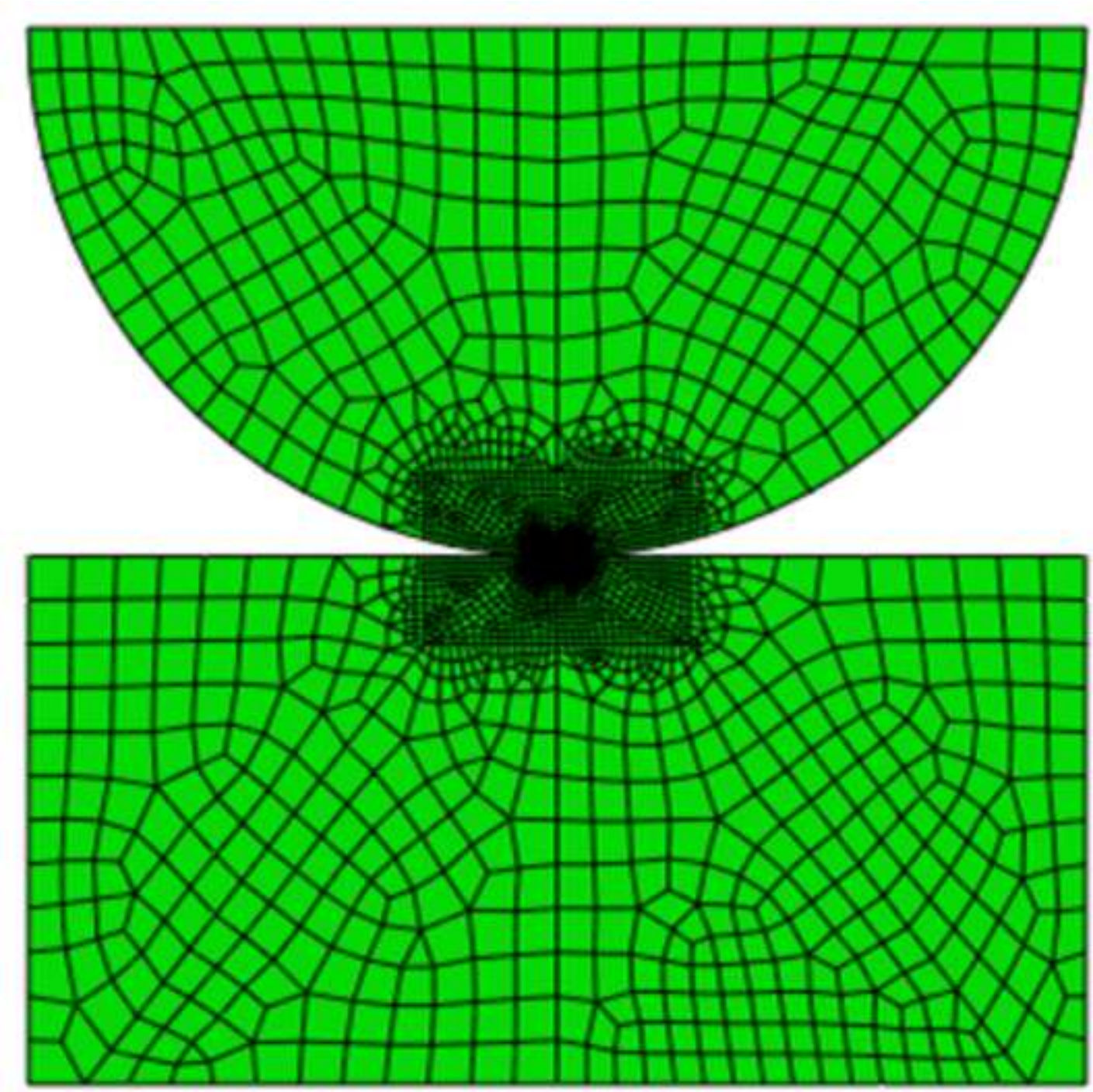

Figure 10(a)
Click here to download high resolution image

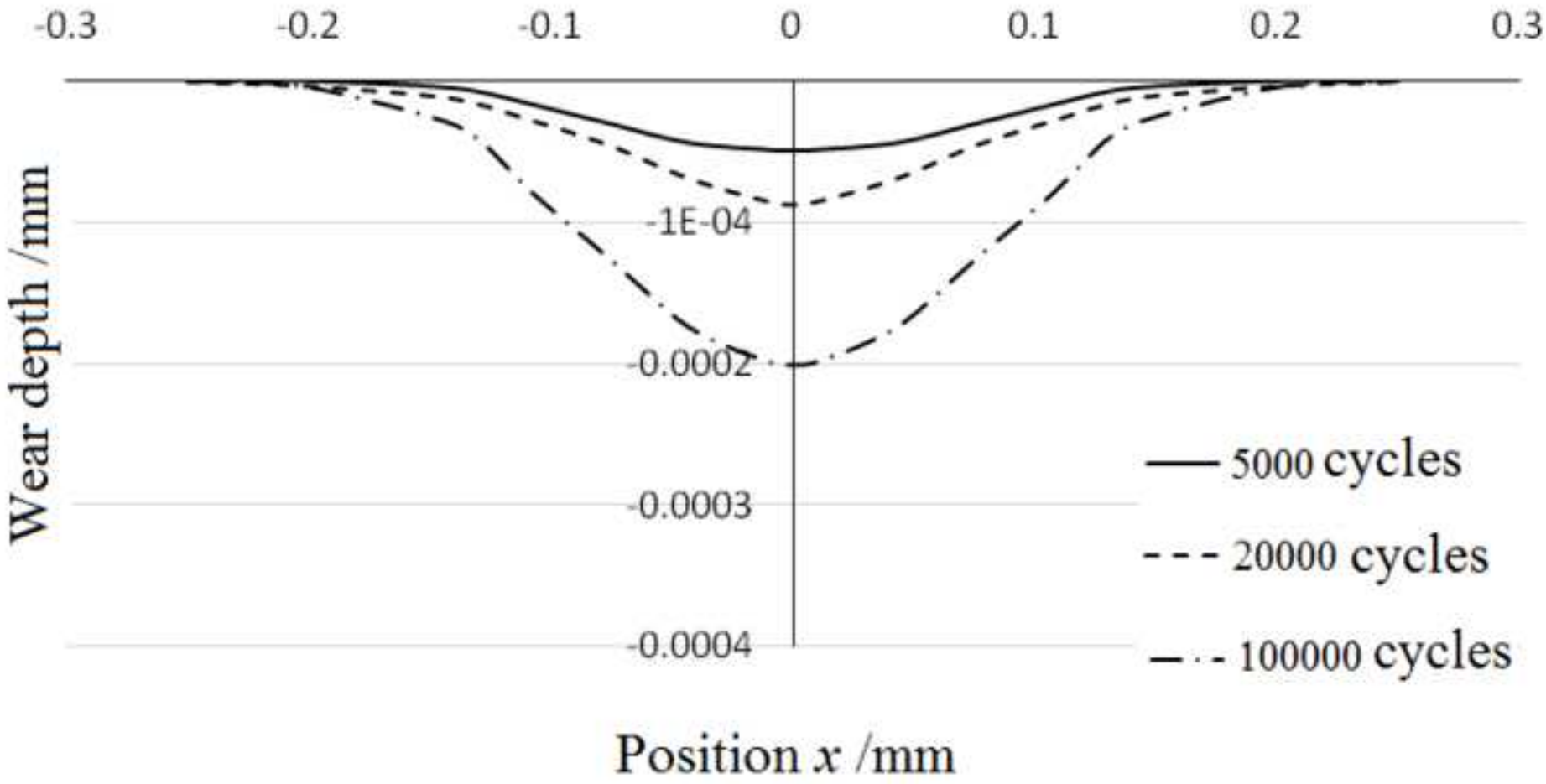

Figure 10(b)
Click here to download high resolution image

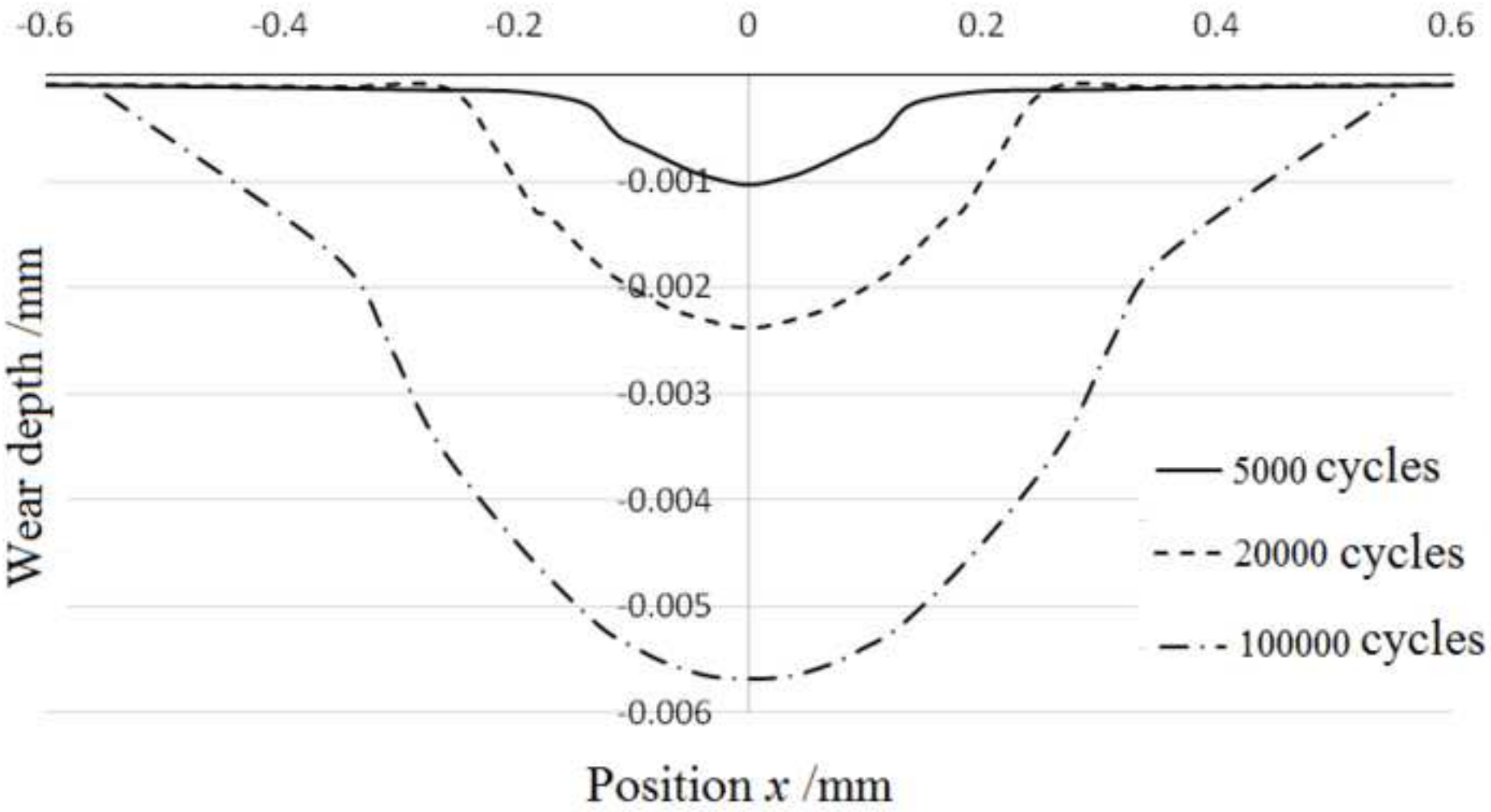

Figure 11(a)

Click here to download high resolution image

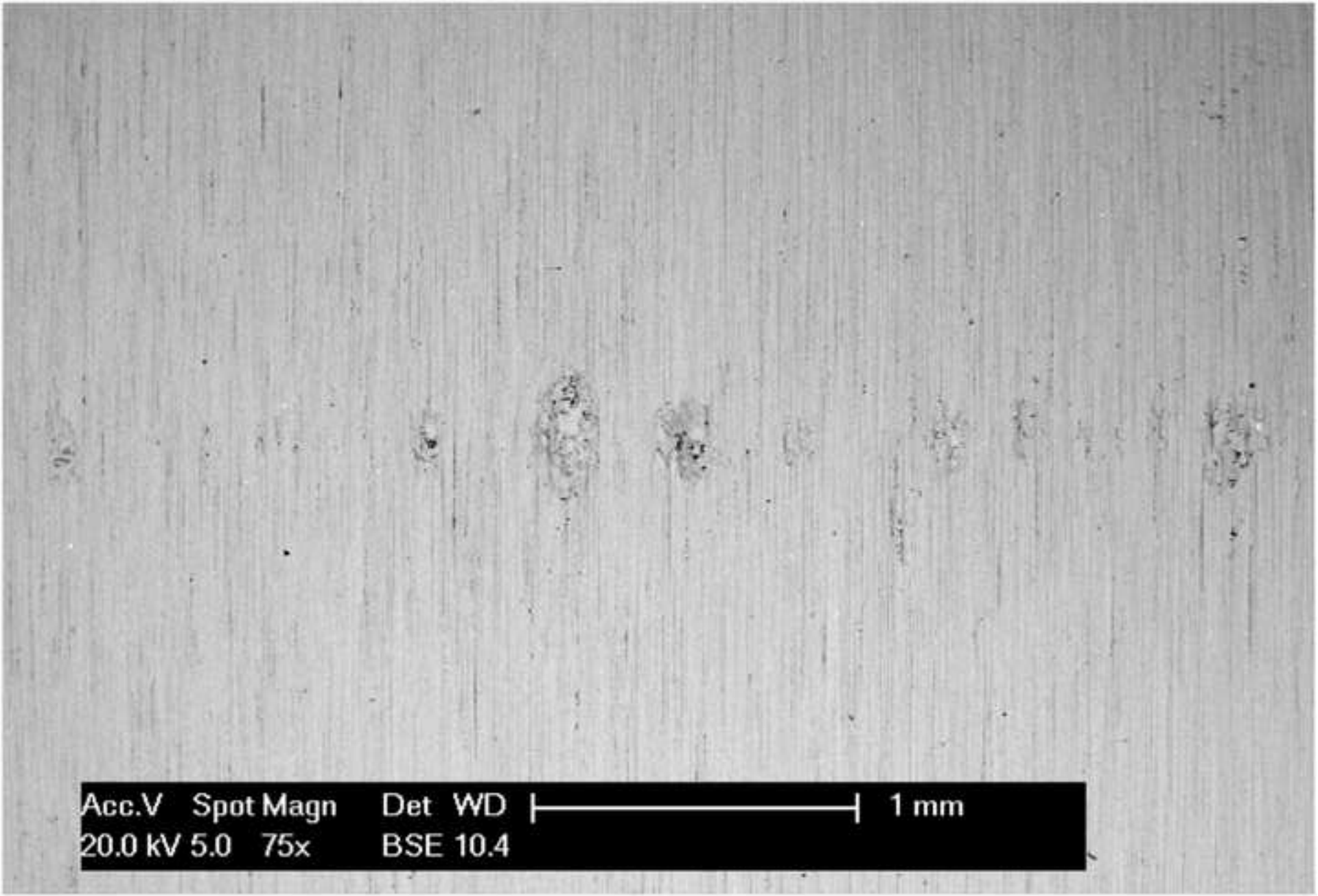

Figure 11(b)

Click here to download high resolution image